

# Spectrally multimode squeezed states generation at telecom wavelengths

Victor Roman-Rodríguez<sup>1,2</sup>\*, David Fainsin<sup>1</sup>, Guilherme L.

Zanin<sup>1</sup>, Nicolas Treps<sup>1</sup>, Eleni Diamanti<sup>2</sup>, and Valentina Parigi<sup>1</sup>

<sup>1</sup>*Laboratoire Kastler Brossel, Sorbonne Université, ENS-Université PSL,  
CNRS, Collège de France, 4 place Jussieu, Paris F-75252, France*

<sup>2</sup>*Sorbonne Université, LIP6, CNRS, 4 place Jussieu, 75005 Paris, France*

(Dated: June 14, 2023)

We report on the experimental demonstration of a source that generates spectrally multimode squeezed states of light over the infrared C-Band. This is achieved using a single-pass Spontaneous Parametric Down Conversion (SPDC) process in a periodically-poled KTP waveguide that is pumped with the second harmonic of a femtosecond laser. Our measurements show significant squeezing in more than 21 frequency modes, with a maximum squeezing value over 2.5 dB. Moreover, we demonstrate multiparty entanglement across 8 individual frequency bands by measuring the covariance matrix of their quadratures. Finally, we use reconfigurable mode-selective homodyne detection to mold the output into cluster states of various shapes. This result paves the way for the implementation of continuous variable quantum information protocols at telecommunication wavelengths, with applications in multiparty, entanglement-based quantum communication and computation.

## I. INTRODUCTION

Continuous variable (CV) encoding of quantum information requires the generation of multimode quantum states of light with tailored spectral, spatial and temporal mode properties [1, 2]. In particular, measurement-based protocols are based on the possibility of deterministically generating large multimode entangled states, where entanglement is established between amplitude and phase quadratures of different light modes [3–7]. This in turn requires the generation of a large number of squeezed modes.

Second-order nonlinear waveguides are currently largely explored to generate tailored squeezed modes: single-mode over a large bandwidth [8–10], temporally multiplexed [11], and both spectrally and temporally multiplexed [12].

Particular effort has been devoted to generate squeezed sources at telecommunication wavelengths. Single-mode quantum states with significant squeezing [13, 14], on-chip few-mode squeezed states [15, 16] and micro-comb structures have been shown [17]. Recent results on single-mode squeezing generation in nonlinear waveguides have been reported in a regime where optical communication technologies can be exploited [8], where it is possible to have quantum state transmission through fibers over long distances [18] and sensing [19].

Here we demonstrate the generation of a vacuum squeezed field in the near infrared C-Band that is intrinsically spectrally multimode, *i.e.*, a system that cannot be reduced to a single squeezer acting on a specific spectral mode, but that involves many squeezers acting on different (orthogonal) spectral modes. This implies that

the many spectral modes can be directly shaped, via linear optics transformations, into entangled networks of the same number of nodes without mixing them with extra vacuum field states, thus not degrading the squeezing and/or entanglement correlations. The networks built in this way can be easily tailored in our setup via mode-selective homodyne detection [4], and their quality can be characterized via the squeezing level of their so-called nullifier operators. We can also independently check entanglement correlations between different individual frequency bands, by measuring the full quadrature covariance matrix for 8 different bands. A Positive-Partial-Transpose (PPT) criterion can be used as an indication of entanglement over all the possible band bipartitions.

Both intra-band entanglement and cluster structures can be used for frequency-multiplexed QKD [20] and entangled-based multiparty quantum communication protocols [21].

Moreover, the demonstrated source, being pumped with a pulsed laser in a single-pass configuration, is compatible with simultaneous spectral and temporal (pulse-based) multiplexing [22] as well as mode-selective non-Gaussian operations [23]. This fact makes the source appealing for the generation of scalable 3-dimensional entangled structures to be used in measurement-based quantum computing [24].

The paper is structured as follows: in Section II we briefly summarize the theoretical description of the generation of the multimode quantum states via SPDC in type 0 nonlinear waveguides [25]. We also describe our scheme for the experimental setup used in this work. In Section III, we show the experimental results, covering multimode squeezing, covariance matrix in the basis of equidistant frequency bands (that we call frexel basis, [26]), and squeezing in the nullifiers of certain cluster states. We conclude this work with a summary in Section IV.

\* victor.roman@icfo.eu; Currently with ICFO - Instituto de Ciencias Fotonicas, The Barcelona Institute of Science and Technology, 08860 Castelldefels, Barcelona, Spain

## II. EXPERIMENT DESCRIPTION

### A. Multimode SPDC

We proposed the generation and engineering of CV multipartite entangled states of light in the frequency domain via SPDC, using nonlinear waveguides, in [25]. Details about the theoretical considerations can be found there and in the references within. In summary, we investigated the properties of the joint spectral amplitude (JSA):

$$J(\omega_s, \omega_i) = \sum_k \lambda_k h_k(\omega_s) g_k(\omega_i), \quad (1)$$

where  $\omega_{s/i}$  is the signal/idler frequency,  $\lambda_k$  are the Schmidt coefficients and  $h_k(\omega_s)$  ( $g_k(\omega_i)$ ) are the signal (idler) frequency modes composing the signal (idler) field after the interaction. Given that the JSA contains all the frequency information of our states, the output signal and idler fields can be described with the modes:

$$\begin{aligned} \hat{A}_k^\dagger &= \int d\omega_s h_k(\omega_s) \hat{a}^\dagger(\omega_s) \\ \hat{B}_k^\dagger &= \int d\omega_i g_k(\omega_i) \hat{b}^\dagger(\omega_i), \end{aligned} \quad (2)$$

which define the sometimes called *supermode basis* [27]. The Hamiltonian describing the interaction in this basis takes the form:

$$\hat{H} = \sum_k^N \lambda_k \hat{A}_k^\dagger \hat{B}_k^\dagger + \text{h.c.} \quad (3)$$

Evolution under this Hamiltonian is known to produce  $N$  independent pairs of completely entangled modes (EPR pairs). In [25], we focused on the EPR pair multimode field as a starting point for the generation of the more general cluster states in the context of type II SPDC. In the experiment described here, for practical reasons, we work instead with the type 0 process in the degenerate case, *i.e.*, when the signal and idler modes are identical,  $\hat{A}_k = \hat{B}_k$ , and hence there is a unique output field. In this case the Hamiltonian of Eq. (3) reduces to:

$$\hat{H} = \sum_k^N \lambda_k \left( \hat{A}_k^\dagger \right)^2 + \text{h.c.} \quad (4)$$

Evolution under this Hamiltonian produces a multimode field with  $N$  independent squeezed states. Therefore, we can take as the experimental signature of the generation of these states the squeezing levels of our multimode output field. Each individual squeezed mode can be addressed experimentally via coherent (homodyne) detection. Indeed, since homodyne detection is a projective measurement, interference with a properly spectrally shaped Local Oscillator (LO) gives access to the noise properties of the individual modes under study [26].

Once the squeezing levels are characterized, the generation of a particular cluster state with up to  $N$  nodes can be obtained by performing an adequate unitary transformation [28, 29]. This can be done by adding to the experimental setup a passive optical circuit performing the unitary operation, or equivalently, changing appropriately the LO shape to access directly the modes composing the cluster state with homodyne detection [1, 4].

### B. Experimental Setup

The experimental setup for generating the multimode squeezed state is depicted schematically in Fig. 1. A broadband fiber femtosecond laser (characteristics: bandwidth  $\sim 55$  nm, pulse width  $\sim 57$  fs, repetition rate 100 MHz, power  $\sim 500$  mW, centered at 1560 nm), is partly directed to a periodically poled Lithium Niobate (ppLN) crystal, engineered to produce the second harmonic frequency. After the ppLN we obtain light with a bandwidth of  $\sim 2$  nm, centered at 780 nm. This field is then coupled to a single(spatial)-mode, rectangular, nonlinear, periodically poled Potassium Titanyl Phosphate (ppKTP) waveguide[30] that down converts the second harmonic field to the C-band telecom wavelengths and generates the multimode squeezed states.

On the other side, a big fraction of the original power from the laser is sent to a pulse shaper in order to generate a spectrally configurable LO. The signal field from the waveguide and the LO are mixed and directed to separate photodiodes, whose electrical outputs are subtracted to obtain the homodyne signal.

We constructed the pulse shaper by diffracting the wavelength components of our input field using a grating, and directing them to a Spatial Light Modulator (SLM), where the light is reflected back and recombined in a similar grating (so called 4f configuration)[31]. In the SLM screen, each pixel, and hence, each frequency component of the field, can be addressed individually, resulting in a spectrally shaped pulse at the output. We used a home-made interface in Python to control the different masks applied to the pulse shaper.

The LO is then passed by another ppKTP waveguide (identical in dimensions) before mixing it with the quantum signal. This is done to spatially match the LO and the signal, effectively decreasing losses in the detection.

We performed numerical simulations in advance in order to predict the properties of the independent squeezed modes following [25]. Details about these numerical simulations and about the characterization of our waveguides can be found in Appendix A.

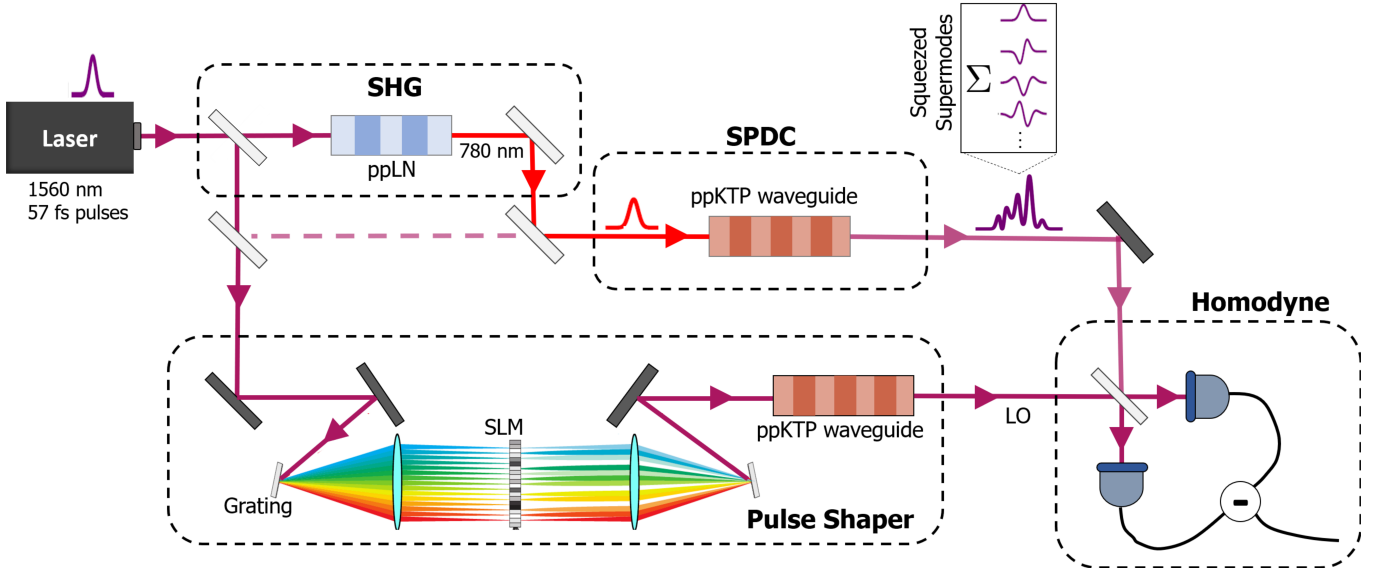


FIG. 1. **Experimental scheme for the generation of the multimode states.** A telecom wideband (bandwidth around 55 nm) pulsed laser is up converted to its second harmonic with a ppLN crystal and then coupled to a nonlinear ppKTP waveguide. Type 0 SPDC interaction generates independent squeezing in a set of frequency modes. Each mode is addressed individually with homodyne detection, where the LO is shaped spectrally with the use of a pulse shaper. For more details see text.

### III. EXPERIMENTAL RESULTS

#### A. Multimode Squeezing

Fig. 2 summarizes the squeezing values obtained in each of the measured modes, where the shot noise stands as reference (0 dB). The quadrature noise was measured as a function of the relative phase between the signal and the LO, for different LO spectral shapes, via a spectrum analyzer. The relative phase is modulated in time thanks to a piezoelectric mirror in the LO optical path. We first performed the experiment by projecting the states into the family of Hermite-Gauss (HG) modes. The particular family we used, derived from our numerical simulation, is defined by a fundamental HG<sub>0</sub> mode with 45 nm of FWHM (in amplitude).

The Sqz (squeezing) and ASqz (antisqueezing) values of Fig. 2 are the minimal and maximal values of the quadrature noise measured via averaging on scans of several phase-periods from the spectrum analyzer.

The asymmetry between squeezing and antisqueezing levels (typical values are -1.0 dB for squeezing and 1.4 dB for antisqueezing), is attributed to experimental optical losses.

The main loss source is the non-optimal spatial mode-matching between the signal and LO optical modes. We characterize it by measuring the visibility of fringes between the LO and a small fraction of telecom light coupled into the waveguides. The associated quantum efficiency scales quadratically with the measured visibility

(other contributions to the global quantum efficiency in the homodyne setup are defined in Appendix B).

In order to match the spatial modes of LO and signal, we inserted, in the LO path, a waveguide identical to the one used for the generation of the signal. The overall visibility in such a configuration, which is the one of the measurements in Fig. 2, reaches the value of 77%.

We explain the non-ideal visibility by residual differences between the spatial modes of the signal and the LO. This can be due to inhomogeneities in the two waveguide structures that are known to appear when the waveguide is long ( $\sim$  cm scale).

Fig. 2 also shows the spectral shapes set in the LO pulse shaper to measure the corresponding squeezing values. A detrimental effect in our setup is what we call optical clipping, which arises due to the limited size of the cylindrical mirror responsible for focusing the light beam onto the SLM for pulse shaping. Since the beam comes from a refractive element (a grating), some wavelengths at the extremes of the spectrum are therefore cut off. Due to this effect, the LO spectral extremes cannot be used are not in homodyne detection (the corresponding clipped regions from the different modes are shown in red in Fig. 2). We would then expect larger values for the measured squeezing levels if the full spectrum was experimentally available.

It is also worth mentioning that due to the optical clipping, the cut HG modes in which we project our state are technically not orthogonal anymore. The dimension of the subspace spanned by the modes shown in Fig. 2 is nevertheless close to 21 HG modes (details can be found

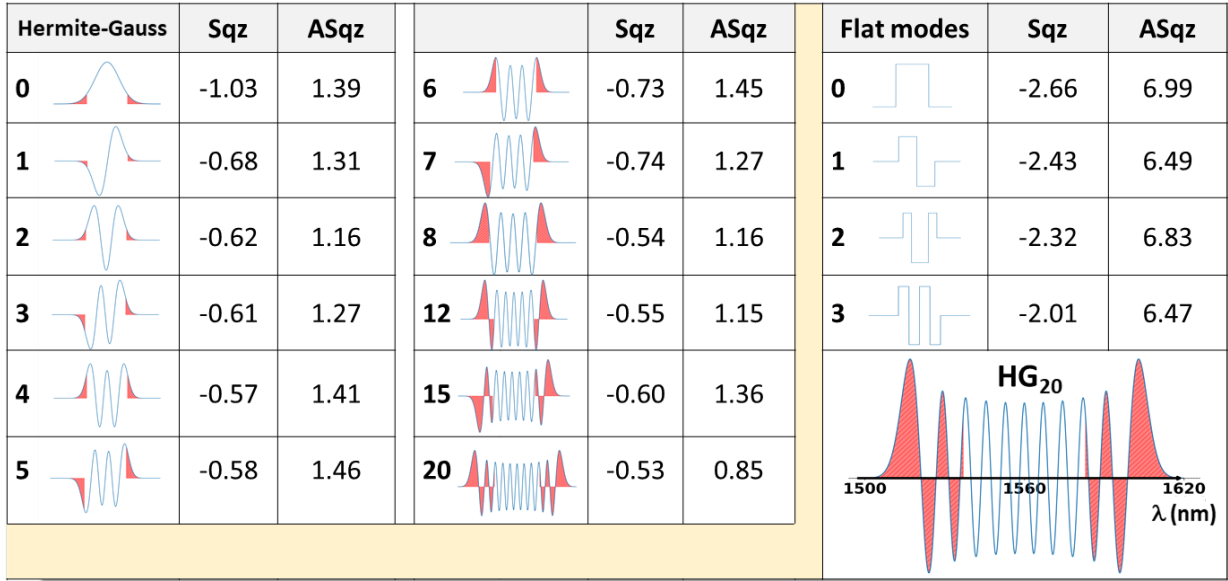


FIG. 2. **Multimode Squeezing Curves.** Left : We summarize, for each Hermite-Gauss mode (supermode) the quantity of squeezing and anti-squeezing measured experimentally. The shot noise stands as reference (0 dB). For each mode, the red area represents the part of the spectrum not accessible to our Local Oscillator. Top Right : Measurement in the ‘flat’ mode basis (for details see text). Down right: A zoom on the necessary spectral range for mode HG20.

in Appendix D, where we calculate it to be around 18).

Furthermore, we projected the states into a basis of a form of orthogonal and flattened HG modes that we call *flat* modes. For such modes we observed larger squeezing values - with more than 2 dB of squeezing up to the 4th mode - than for the HG modes. The flat modes and their squeezing level are shown in the right side of Fig. 2, as well as in Appendix E. This result implies that the HG basis shown on the left side of Fig. 2 is not the family of supermodes, since those should be the most squeezed modes in the system.

Further evidence in this direction is given by the covariance matrix measurements in the next section, showing that the spectral widths of the theoretically predicted HG modes are probably underestimated.

We therefore expect that the measured squeezing values in Fig. 2 constitute a lower bound for the potential squeezing that can be achieved with larger mode-matching visibilities and without optical clipping. This is also witnessed by the significant asymmetry in the squeezing and antisqueezing values measured in the flat mode basis.

To summarize the above discussion, Fig. 2 demonstrates the experimental realization of an optical multimode squeezed state composed of at least 21 frequency modes, with reasonable margin for improvement, and that can be used for the quantum information protocols.

## B. Covariance Matrix measurement

In order to check the presence of entanglement, *i.e.*, quantum correlations, in our multimode state, we measured the state in different basis from the one of the supermodes [32]. In particular, we used the so-called *frexel* basis, which is composed of a number of equally spaced frequency bands covering the total spectrum of the LO. This is a suitable basis, not only because it is easily accessible via the shaping capability of the LO, but also because the frexel modes can be easily spatially separated via dispersive elements and sent to different locations, which is necessary for multiparty quantum protocols. We therefore measured the covariance matrix that characterizes our gaussian state, in the frexel basis, using 8 equally spaced frequency bands.

The covariance matrix is shown in Fig. 3. Under the reasonable assumption of a non-chirped pump, we expect no correlations between the different position,  $q_i$ , and momentum,  $p_j$ , quadrature components and hence zero value for the symmetrized expectation values of the form  $q_i p_j$  [27, 33]. We then measure only the subgroups of  $q_i q_j$  or  $p_i p_j$  quadratures. The results are shown in the left of Fig. 3. The non-zero off-diagonal elements in the data show the presence of correlations between the frequency bands defining the 8 freixels in our state. This can be associated to the entanglement between the frequency bands that can be tested via the positive partial transpose (PPT) criterion [34] (see Appendix G for more details). We obtained violation of the PPT criterion for all of the possible bipartitions of our system.

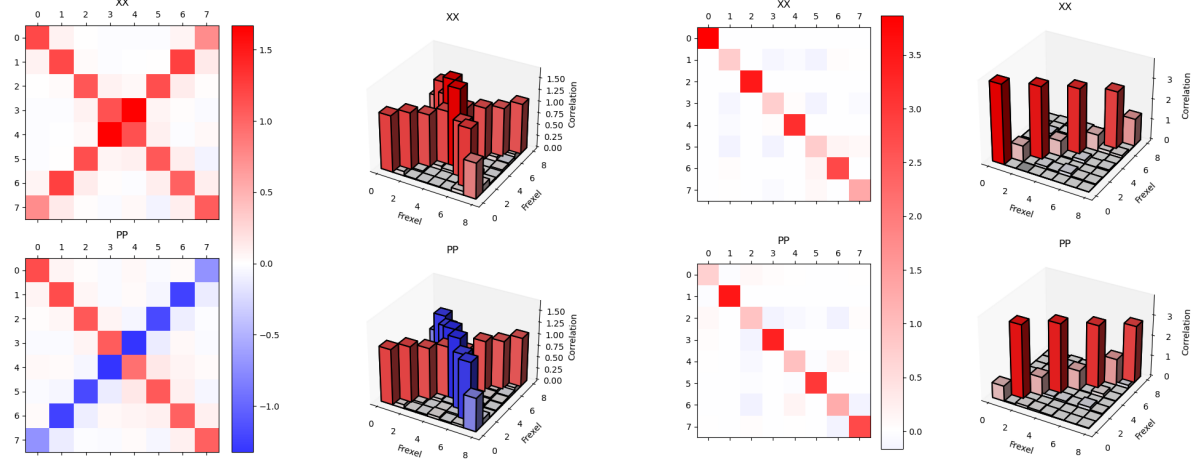


FIG. 3. **Reconstructed covariance matrix.** The covariance matrix on the left is obtained by measuring the multimode state in the frexel basis, using 8 frequency bands. On the right, we show a numerical diagonalization of the measured covariance matrix for recovering the squeezed supermodes.

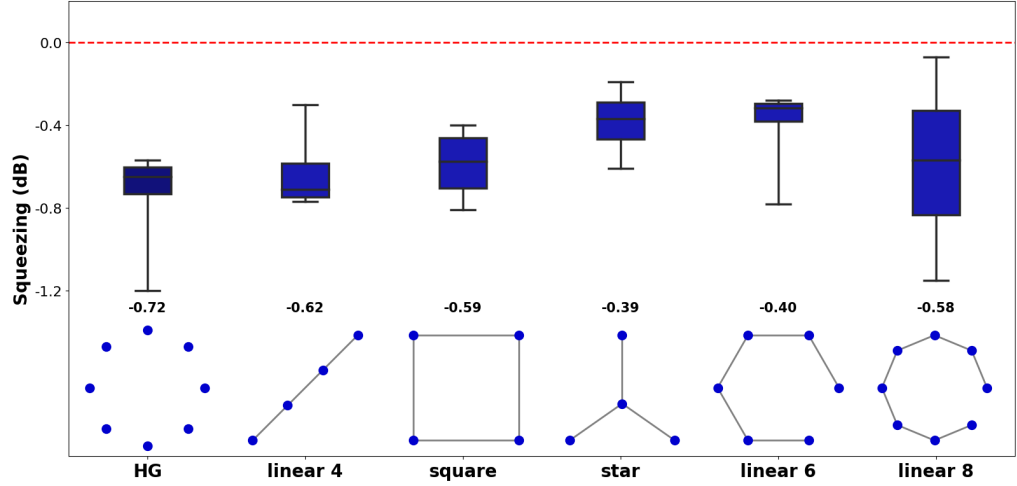


FIG. 4. **Cluster state generation.** The boxplots sum up the maximum squeezing value for the first HG modes and the nullifiers of different cluster state size and topologies. The values indicate the mean nullifiers's squeezing value.

On the right of Fig. 3, we perform a numerical diagonalization of the measured covariance matrix to recover the eigenmode basis, where no entanglement is present. Thus we expect these eigenvectors to resemble discretized versions of the supermodes, with eigenvalues related to a squeezing level value over the frequency band composing the frexel. Overall, the numerical eigenvectors obtained in the diagonalization are in good agreement with the theoretical prediction of approximate Hermite-Gauss modes, except that their spectral widths are larger than the theoretically predicted modes. This is consistent with

the measurement of larger squeezing values in the flat modes basis rather than in the theoretically derived HG mode basis, as shown in the previous section.

The eigenmodes and eigenvalues from the diagonalization of the covariance matrix can be found in Appendix F.

### C. Cluster State Generation

Finally, we used the experimental setup for the deterministic generation of some few-node cluster states, as a proof of principle on the versatility of the source.

We probe the generation of the cluster states by measuring squeezing in the nullifiers that characterize a specific adjacency matrix, *i.e.*, a particular topology defining the graph. Changing from one topology to another can be achieved by appropriately changing the mask on the pulse shaper [35]. The nullifiers,  $\{\hat{\delta}_i\}$ , of a particular graph with quadratures operators for the nodes denoted  $\hat{q}_i$  and  $\hat{p}_i$  are written as:

$$\hat{\delta}_i = \hat{p}_i - \sum_j V_{ij} \hat{q}_j, \quad (5)$$

where  $V_{ij}$  are the elements of the adjacency matrix defining the cluster state, which is known in advance[28]. Furthermore, the quality of the probed cluster state can be qualitatively obtained by the amount of squeezing measured in the nullifiers.

We measured 4-node cluster states with different topologies and whose nullifier's level of squeezing is summarized in Fig. 4 via statistical box plots for each cluster topology. Additionally, we show that all nullifiers are squeezed below the shot noise up to an 8-mode linear cluster. This proves the generation of the cluster states. We leave further source optimization for future studies and experiments.

## IV. CONCLUSION

In this work we report on a deterministic source of multimode quantum states of light generated via type 0 SPDC in a nonlinear ppKTP rectangular waveguide. We measured up to 21 squeezed optical spectral modes in the HG basis and over 2 dB of squeezing for four spectral *flat* modes. We measured and diagonalized the covariance matrix in the frexel basis and demonstrated the realization of different cluster states topologies, characterizing them with the squeezing in their nullifier operators. The quality of the resource can be enhanced by improving the signal-LO mode-matching and the optical configuration of the pulse shaper, both within reach of current technology. The demonstrated source can be used to implement entanglement based quantum communication protocols and to build scalable resources for quantum computing at telecom wavelenghts.

## ACKNOWLEDGMENTS

This work was supported by the European Research Council under the Consolidator Grant COQCooN (Grant No. 820079).

## Appendix A: Numerical simulation of the multimode state in our experimental configuration

Numerical simulations were performed in order to predict the properties of the independent squeezed modes at the output of the waveguide. Given the experimental values measured from the second harmonic field (hence the pump to the ppKTP waveguide), and the chosen waveguide dimensions (3 by 3  $\mu\text{m}$  and 15 mm in length), the results are shown in Fig. 5. A number of about 34 modes is expected with the Schmidt distribution,  $\{\lambda_k\}$ , shown in the figure. The first three frequency modes, similar to Hermite-Gauss modes, are also shown. For more details about the numerical simulation of the nonlinear waveguides and how the experiment was designed, see [25].

## Appendix B: Waveguide Characterization

The characterization of our waveguides was performed by coupling them to the C-band wavelength (1560 nm). A measurement of the spectrum of the second harmonic field produced by the C-band input gives an estimate on the homogeneity of the waveguide along the propagation direction (a sinc-like function is to be measured, which is the response to a square nonlinear profile by the Fourier transform, expected from a homogeneous structure). The amount of second harmonic produced from the telecom input gives an estimate on the nonlinear coefficient of the waveguide, that is fitted from data in the next section. Finally, a measurement of the spatial profile of the output telecom light can be compared with a numerical simulation (in our case with a finite element method, [36]) to check the single-spatial-mode feature of the waveguides, and the deviation from the expected fundamental mode propagating in the actual structure.

The homodyne measurement was performed with a home-made detector, including the two photodetectors and the transimpedance circuit outputting the homodyne electrical signal. The total homodyne efficiency,  $\eta_h$ , can be decomposed in the following terms:

$$\eta_h = \eta_{\text{PD}} \cdot \eta_{\text{el}} \cdot \eta_{\text{opt}} \cdot \eta_{\text{mod}}, \quad (\text{B1})$$

where  $\eta_{\text{PD}}$  is the photodetector's efficiency (around 85% in our case),  $\eta_{\text{opt}}$  is related to the optical losses in the homodyne circuit (near unity in our case),  $\eta_{\text{mod}}$  is the mode matching efficiency, *i.e.*, how close are the LO and the signal in terms of polarization, spatial and temporal profile when interfering, and  $\eta_{\text{el}}$  is the electronic efficiency.

The electronic efficiency can be written as  $\eta_{\text{el}} = 1 - 1/\text{SNR}$  [37], with SNR the signal to noise ratio, *i.e.*, the ratio between the shot noise at a certain input intensity and the value in the absence of any input signal (electronic noise). We measured the best signal-to-noise ratio (also called clearance, if one measures it in dB) at a demodulation frequency of 2 MHz, where the clearance was about 20 dB at 2 mW of input power.

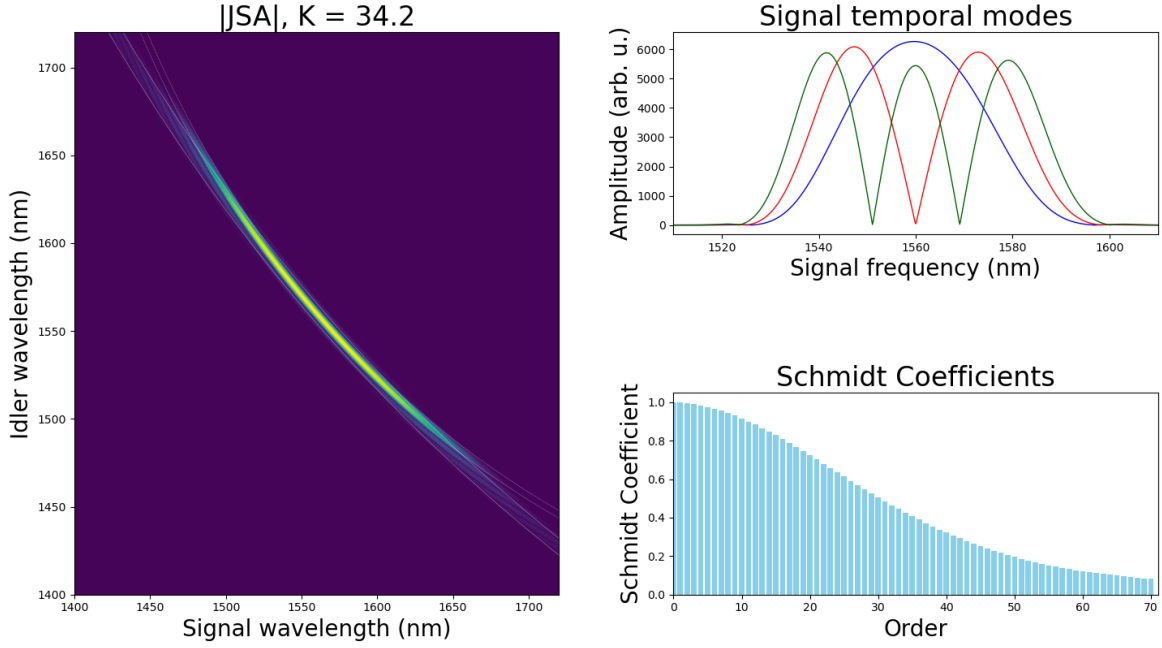


FIG. 5. Numerical simulation of the independent squeezed states. Left: JSA function, Right: First three frequency modes, resembling Hermite-Gauss and the distribution of the Schmidt coefficients for every supermode.

The mode-matching efficiency was limiting the amount of available squeezing in our experiment and it is discussed in the main text.

### Appendix C: Phase Sensitive Amplification Results

Before measuring the multimode squeezing curves shown in the main text, we built a degenerate Optical Parametric Amplifier, or OPA, by pumping the waveguide with a relatively intense seed field at telecom wavelengths (taken directly from the ultrafast laser) and a pump field (from our second harmonic ppLN crystal at 780 nm).

The phenomenon of parametric amplification can be observed as a modulation of the seed amplitude at the output of the waveguide, depending on the relative phase between the seed and the pump fields. This measurement allows us to show the existence of parametric gain in our waveguides, which is a precondition of squeezing generation, even though the levels of multimode squeezing cannot be predicted in this way.

The extrema of the parametric gain,  $G_{\pm}$ , can be approximated, for a single-mode OPA, as [38, 39]:

$$G_{\pm} \sim \exp(\pm 2\sqrt{\eta_{PSA}P}), \quad (C1)$$

where  $P$  is the pump power and  $\eta_{PSA}$  is the parametric efficiency. Ideally, the minimum deamplification,  $G_-$ ,

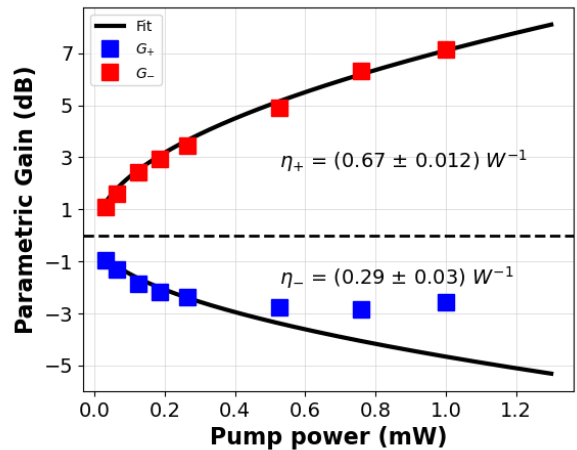


FIG. 6. Parametric gain vs pump power. Extrema in the modulation of the amplitude for the degenerate OPA, fit to Eq. (C1) gives the parametric efficiency, related to the total squeezing level.

should be symmetric with respect to  $G_+$ , although a disparity between the two has been reported when using pulsed lasers, and attributed to a distortion of the spatial or temporal profile inside the nonlinear material. The

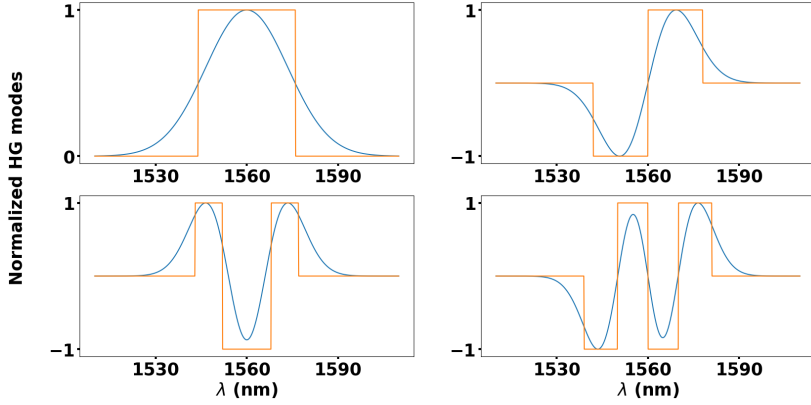


FIG. 7. First 4 Hermite-Gauss modes measured (blue) and the corresponding spectral flat modes obtained from them (orange).

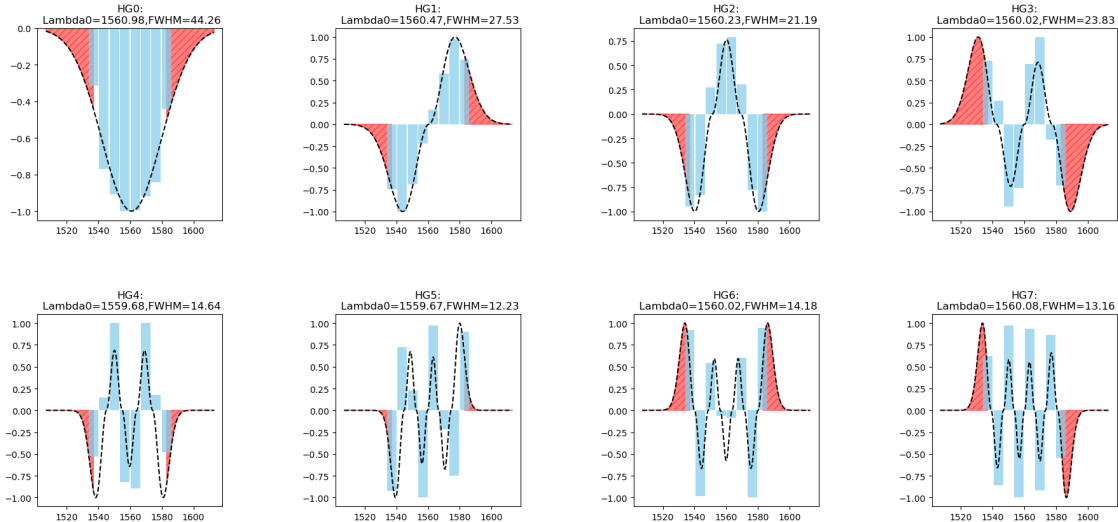


FIG. 8. **Eigenmodes of the covariance matrix** The amplitudes of the eight eigenmodes were plotted and fitted with Hermite Gauss functions. The wavelength outside of the Local Oscillator bandwidth was emphasized by marking it with a red hatched area.

disparity appears at sufficiently high power density in the material.

Fig. 6 shows the parametric gain measured as a function of the pump power. The data fits well Eq. (C1) and gives two values for the parametric efficiency due to their asymmetry. However, a measurement of the second harmonic efficiency in the same nonlinear waveguide gives an efficiency of  $\eta_{\text{SHG}} = 0.33 \text{ W}^{-1}$ , which is in good agreement with the extracted parametric efficiency for the deamplification.

The conclusion of the phase sensitive experiment is that, at pump powers of few mW, we can expect at least some dB of total squeezing in our multimode states, which are the measured values showed in the main text.

#### Appendix D: Independent Hermite-Gauss modes

As discussed in the main text, due to optical clipping, the 21 clipped Hermite-Gauss modes implemented in the experiment were not exactly orthogonal, and therefore the actual number of measured supermodes is expected to be lower than 21. This number depends on the dimensionality of the vector space spanned by the non-orthogonal modes. In order to account for that, we evaluate the rank of the matrix composed by these modes performing a singular value decomposition on the set of 21 vectors. The non-zero singular values count the number of linearly independent modes and hence the dimension of the space we are looking for. The singular values resulting from the decomposition is summarized in Ta-

ble I.

TABLE I. Singular values obtained from clipped Hermite-Gauss modes used in the experiment.

Sing. Val.	0	1	2	3	4	5	6	7	8	9
	1.42	1.40	1.31	1.28	1.21	1.19	1.18	1.12	1.09	1.08
Sing. Val.	11	12	13	14	15	16	17	18	19	20
	0.99	0.97	0.94	0.90	0.84	0.60	0.30	0.08	0.02	0.005

Since this is a numerical computation, we need a somewhat arbitrary criterion to give a whole number indicating the dimension of our vector space from this result. In our case, we obtain the dimension of the vector space by accounting for singular values that are at least 10% of the highest one. This criterion gives us 18 linearly independent modes. The value being close to the 21 Hermite-Gauss modes indicates that the optical clipping did not have a large impact in reducing the dimensionality of the modes measured in the experiment.

#### Appendix E: Flat mode basis

The spectral flat mode basis discussed in the main text is constructed to be orthogonal, taking advantage of even and odd symmetries for the subsequent mode functions. It was specifically designed to roughly resemble the first 4 Hermite-Gauss modes, so that the spectral width of each flat mode was obtained by minimizing the  $l^2$  norm distance to the corresponding Hermite-Gauss mode counterpart. Fig. 7 shows the 4 flat modes constructed and implemented in the experiment, together with the first 4 Hermite-Gauss modes from the supermode basis.

#### Appendix F: Eigenmodes from the diagonalization of the covariance matrix

The numerical diagonalization of the covariance matrix performed in the main text gives back the eigenmode basis where there are no quantum correlations, *i.e.*, the supermode basis discussed in the text. For additional information concerning the reconstruction of the covariance matrix see [12].

We therefore expect the numerical eigenmodes to resemble discretized versions of the quasi-Hermite-Gauss supermodes found in our numerical simulations from theory.

Fig. 8 shows the numerical eigenmodes obtained after the diagonalization. In general, the supermode shapes are in very good agreement with the expected theoretical Hermite Gauss modes. The bandwidth of every Hermite-Gauss is systematically higher than the theoretical value, which together with the optical clipping in the pulse shaper and the LO bandwidth could be causing the degradation of the measured squeezed values described in the main text.

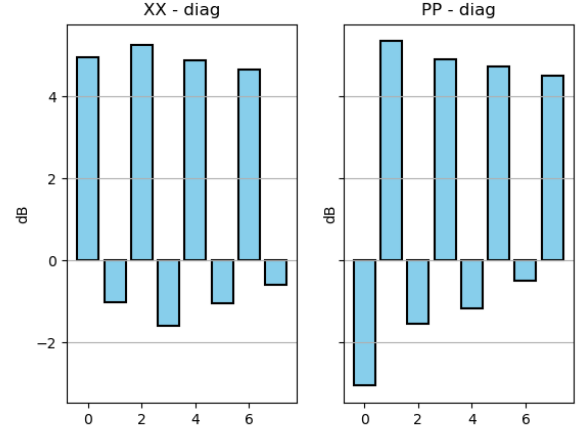


FIG. 9. Squeezing values obtained from the numerical diagonalization of the covariance matrix in the frequency basis. The modes have been arranged in decreasing order of anti-squeezed quadratures, and the first eigenmode is squeezed in the  $\hat{p}$  quadrature by convention.

On a technical note, the 55 nm bandwidth of our LO was slightly smaller than the bandwidth of our expected quantum signal. This limits the experimentally accessible modes if the wavelengths outside the LO bandwidth are involved in the spectral features of the supermode. This effect is noticeable for high-order modes, which are the most broadband. In Fig. 8, the red area highlights the wavelength range that was not accessible with our LO bandwidth.

Please also note that the eigenvalues of the covariance matrix are directly related to the expected squeezing levels of each eigenmode. Fig. 9 shows the eigenvalues obtained in the diagonalization, which are consistent with those values directly measured in the supermode basis in the main text.

#### Appendix G: Peres–Horodecki (PPT) criterion

As explained in the main text, the Positive Partial Transposition (PPT) criterion can be applied to determine whether quantum correlations are present in our data of the covariance matrix.

The PPT criterion is based on the fact that given a density matrix defining a quantum state, the partial transpose matrix of two possible bipartitions of the density matrix has to be positive defined for the two bipartitions being separable. The criterion applied to continuous variable systems can be found, for example, in [34]. This theorem applies to the covariance matrix since it completely defines any gaussian state.

In our case, given that we have an 8x8 matrix in our frexel basis, we have a total of 127 possible bipartitions. For each bipartition, we can define the minimum eigen-

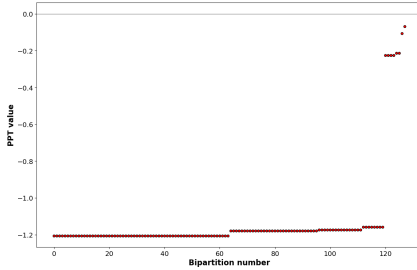


FIG. 10. PPT values computed for all 127 possible bipartitions. The results show that all of the values are negative, thereby indicating the non-separability of the state.

value of the partial transpose matrix as the PPT value, indicating quantum correlations if negative.

Fig. 10 shows the PPT value for the different bipartitions of our covariance matrix, showing the violation of the PPT criterion, *i.e.*, negativity in the partial transpose matrix, in all of them.

More details about the PPT criterion applied to the covariance matrix can be found in [40].

---

[1] J. Roslund, R. Medeiros de Araújo, S. Jiang, and N. Fabre, C. Treps, Wavelength-multiplexed quantum networks with ultrafast frequency combs, *Nature Photonics* **8**, 109–112 (2014).

[2] V. Ansari, J. Donohue, B. Brecht, and C. Silberhorn, Tailoring nonlinear processes for quantum optics with pulsed temporal-mode encodings, *Optica* **5**, 534 (2018).

[3] M. Chen, N. C. Menicucci, and O. Pfister, Experimental realization of multipartite entanglement of 60 modes of a quantum optical frequency comb, *Phys. Rev. Lett.* **112**, 120505 (2014).

[4] Y. Cai, J. Roslund, G. Ferrini, F. Arzani, X. Xu, C. Fabre, and N. Treps, Multimode entanglement in reconfigurable graph states using optical frequency combs, *Nat. Commun.* **8**, 15645 (2017).

[5] S. Yokoyama, R. Ukai, S. C. Armstrong, C. Sornphiphatphong, T. Kaji, S. Suzuki, J.-i. Yoshikawa, H. Yonezawa, N. C. Menicucci, and A. Furusawa, Ultra-large-scale continuous-variable cluster states multiplexed in the time domain, *Nature Photonics* **7**, 982 (2013).

[6] W. Asavanant, Y. Shiozawa, S. Yokoyama, B. Charoensombutamon, H. Emura, R. N. Alexander, S. Takeda, J.-i. Yoshikawa, N. C. Menicucci, H. Yonezawa, and A. Furusawa, Generation of time-domain-multiplexed two-dimensional cluster state, *Science* **366**, 373 (2019).

[7] M. V. Larsen, X. Guo, C. R. Breum, J. S. Neergaard-Nielsen, and U. L. Andersen, Deterministic generation of a two-dimensional cluster state, *Science* **366**, 369 (2019).

[8] A. Inoue, T. Kashiwazaki, T. Yamashima, N. Takanashi, T. Kazama, K. Enbutsu, K. Watanabe, T. Umeki, M. Endo, and A. Furusawa, Toward a multi-core ultrafast optical quantum processor: 43-ghz bandwidth real-time amplitude measurement of 5-db squeezed light using modularized optical parametric amplifier with 5g technology, *Applied Physics Letters* **122**, 104001 (2023), <https://doi.org/10.1063/5.0137641>.

[9] T. Kashiwazaki, T. Yamashima, K. Enbutsu, T. Kazama, K. Inoue, A. Fukui, M. Endo, T. Umeki, and F. A., Over-8-db squeezed light generation by a broadband waveguide optical parametric amplifier toward fault-tolerant ultrafast quantum computers (2023), arXiv: 2301.12658.

[10] R. Nehra, R. Sekine, L. Ledezma, Q. Guo, R. M. Gray, A. Roy, and A. Marandi, Few-cycle vacuum squeezing in nanophotonics (2022), arXiv: 2201.06768v.

[11] H. Tomoda, T. Yoshida, T. Kashiwazaki, T. Umeki, Y. Enomoto, and S. Takeda, Programmable time-multiplexed squeezed light source, *Opt. Express* **31**, 2161 (2023).

[12] T. Kouadou, F. Sansavini, M. Ansquer, J. Henaff, N. Treps, and V. Parigi, Spectrally shaped and pulse-by-pulse multiplexed multimode squeezed states of light (2022).

[13] S. Ast, M. Mehmet, and R. Schnabel, High-bandwidth squeezed light at 1550 nm from a compact monolithic ppktp cavity, *Opt. Express* **21**, 13572 (2013).

[14] T. Gehring, V. Händchen, J. Duhme, F. Furrer, T. Franz, C. Pacher, R. F. Werner, and R. Schnabel, Implementation of continuous-variable quantum key distribution with composable and one-sided-device-independent security against coherent attacks, *Nature Communications* **6**, 8795 (2015).

[15] F. Mondain, T. Lunghi, A. Zavatta, E. Gouzien, F. Doutre, M. D. Micheli, S. Tanzilli, and V. D’Auria, Chip-based squeezing at a telecom wavelength, *Photon. Res.* **7**, A36 (2019).

[16] F. Lenzini, J. Janousek, O. Thearle, M. Villa, B. Haylock, S. Kasture, L. Cui, H.-P. Phan, D. V. Dao, H. Yonezawa, P. K. Lam, E. H. Huntington, and M. Lobino, Integrated photonic platform for quantum information with continuous variables, *Science Advances* **4**, 10.1126/sci-adv.aa9331 (2018).

[17] Z. Yang, M. Jahanbozorgi, D. Jeong, S. Sun, O. Pfister, H. Lee, and X. Yi, A squeezed quantum microcomb on a chip, *Nature Communications* **12**, 4781 (2021).

[18] I. Suleiman, J. A. H. Nielsen, X. Guo, N. Jain, J. Neergaard-Nielsen, T. Gehring, and U. L. Andersen, 40 km fiber transmission of squeezed light measured with a real local oscillator, *Quantum Science and Technology* **7**, 045003 (2022).

[19] R. Domeneguetti, M. Stefszky, H. Herrmann, C. Silberhorn, U. L. Andersen, J. S. Neergaard-Nielsen, and T. Gehring, Fully guided and phase locked ti:ppln waveguide squeezing for applications in quantum sensing, *Opt. Lett.* **48**, 2999 (2023).

[20] O. Kovalenko, Y.-S. Ra, Y. Cai, V. C. Usenko, C. Fabre, N. Treps, and R. Filip, Frequency-multiplexed entanglement for continuous-variable quantum key distribution, *Photon. Res.* **9**, 2351 (2021).

[21] G. Murta, F. Grasselli, H. Kampermann, and D. Bruß, Quantum conference key agreement: A review, *Advanced Quantum Technologies* **3**, 2000025 (2020), <https://onlinelibrary.wiley.com/doi/pdf/10.1002/qute.202000025>.

[22] T. Kouadou, F. Sansavini, A. Matthieu, H. Johan, N. Treps, and V. Parigi, Spectrally shaped and pulse-by-pulse multiplexed multimode squeezed states of light (2022).

[23] Y.-S. Ra, A. Dufour, M. Walschaers, C. Jacquard, T. Michel, C. Fabre, and N. Treps, Non-Gaussian quantum states of a multimode light field, *Nature Physics* **16**, 144 (2020).

[24] J. E. Bourassa, R. N. Alexander, M. Vasmer, A. Patil, I. Tzitrin, T. Matsuura, D. Su, B. Q. Baragiola, S. Guha, G. Dauphinais, K. K. Sabapathy, N. C. Menicucci, and I. Dhand, Blueprint for a Scalable Photonic Fault-Tolerant Quantum Computer, *Quantum* **5**, 392 (2021).

[25] V. Roman-Rodriguez, B. Brecht, S. K, C. Silberhorn, N. Treps, E. Diamanti, and V. Parigi, Continuous variable multimode quantum states via symmetric group velocity matching, *New Journal of Physics* **23**, 043012 (2021).

[26] J. Roslund, R. Medeiros de Araújo, S. Jiang, C. Fabre, and N. Treps, Wavelength-multiplexed quantum networks with ultrafast frequency combs, *Nat. Photon.* **8**, 109 (2014).

[27] G. Patera, N. Treps, C. Fabre, and G. G. J. de Valcárcel, Quantum theory of synchronously pumped type i optical parametric oscillators: characterization of the squeezed supermodes, *Eur. Phys. J. D* **56** (2010).

[28] N. C. Menicucci, S. T. Flammia, and P. van Loock, Graphical calculus for gaussian pure states, *Phys. Rev. A* **83**, 042335 (2011).

[29] G. Ferrini, J. Roslund, F. Arzani, Y. Cai, C. Fabre, and N. Treps, Optimization of networks for measurement-based quantum computation, *Phys. Rev. A* **91**, 032314 (2015).

[30] The waveguides were purchased from the company AdvR.

[31] A. Monmayrant, S. J. Weber, and B. Chatel, A newcomer's guide to ultrashort pulse shaping and characterization, *Journal of Physics B: Atomic, Molecular and Optical Physics* **43**, 103001 (2010).

[32] S. Brausstein and P. van Loock, Quantum information with continuous variables, *Rev. Mod. Phys.* **77**, 10.1103/RevModPhys.77.513 (2005).

[33] F. Arzani, C. Fabre, and N. Treps, Versatile engineering of multimode squeezed states by optimizing the pump spectral profile in spontaneous parametric down-conversion, *Phys. Rev. A* **97**, 033808 (2018).

[34] R. Simon, Peres-horodecki separability criterion for continuous variable systems, *Phys. Rev. Lett.* **84**, 10.1103/PhysRevLett.84.2726 (2000).

[35] P. Van Loock, C. Weedbrook, , and M. Gu, Building gaussian cluster states by linear optics, *Phys. Rev. A* **76**, 10.1103/PhysRevA.76.032321 (2007).

[36] A. B. Fallahkhair, K. S. Li, and T. E. Murphy, Vector finite difference modesolver for anisotropic dielectric waveguides, *J. Lightw. Technol.* **26**, 1423 (2008).

[37] R. Kumar, E. Barrios, A. J. MacRae, E. C. Cairns, E. H. Huntington, and A. I. Lvovsky, Versatile wideband balanced detector for quantum optical homodyne tomography, *Optics Communications* **285**, 5259 (2012).

[38] D. K. Serkland, M. Fejer, R. L. Byer, and Y. Yamamoto, Squeezing in a quasi-phase-matched linbo<sub>3</sub> waveguide, *Opt. Lett.* **20**, 1068 (1995).

[39] T. Umeki, O. Tadanaga, A. Takada, and M. Asobe, Phase sensitive degenerate parametric amplification using directly-bonded ppln ridge waveguides, *Opt. Express* **19**, 6326 (2011).

[40] R. Medeiros de Araújo, J. Roslund, Y. Cai, G. Ferrini, C. Fabre, and N. Treps, Full characterization of a highly multimode entangled state embedded in an optical frequency comb using pulse shaping, *Phys. Rev. A* **89**, 10.1103/PhysRevA.89.053828 (2014).